The Astrophysical Journal Letters, 961:L46 (7pp), 2024 February 1 https://doi.org/10.3847/2041-8213/ad192e
© 2024. The Author(s). Published by the American Astronomical Society.
OPEN ACCESS

A Floor in the Sun's Photospheric Magnetic Field: Implications for an Independent Small-scale Dynamo

E. W. Cliver[1], S. M. White[2], and I. G. Richardson[3,4]
[1] National Solar Observatory, Boulder, CO 80303, USA
[2] Space Vehicles Directorate, Air Force Research Laboratory, Kirtland AFB, Albuquerque, NM 87117, USA
[3] Department of Astronomy, University of Maryland, College Park, MD 20742, USA
[4] Heliophysics Science Division, NASA Goddard Space Flight Center, Greenbelt, MD 20771, USA
Received 2023 September 6; revised 2023 December 14; accepted 2023 December 19; published 2024 January 31

Abstract

Clette recently showed that $F_{10.7}$ systematically approaches a quiet Sun daily value of 67 solar flux units (sfu) at solar minima as the number of spotless days on the Sun increases. Previously, a floor of ∼2.8 nT had been proposed for the solar wind (SW) magnetic field strength (B). $F_{10.7}$, which closely tracks the Sun's unsigned photospheric magnetic flux, and SW B exhibit different relationships to their floors at 11 yr solar minima during the last ∼50 yr. While $F_{10.7}$ approaches 67 sfu at each minimum, the corresponding SW B is offset above ∼2.8 nT by an amount approximately proportional to the solar polar field strength—which varied by a factor of ∼2.5 during this interval. This difference is substantiated by ∼130 yr of reconstructed $F_{10.7}$ (via the range of the diurnal variation of the East-component (rY) of the geomagnetic field) and SW B (based on the interdiurnal variability geomagnetic activity index). For the last ∼60 yr, the contribution of the slow SW to SW B has exhibited a floor-like behavior at ∼2 nT, in contrast to the contributions of coronal mass ejections and high-speed streams that vary with the solar cycle. These observations, as well as recent SW studies based on Parker Solar Probe and Solar Dynamics Observatory data, suggest that (1) the Sun has a small-scale turbulent dynamo that is independent of the 11 yr sunspot cycle; and (2) the small-scale magnetic fields generated by this nonvarying turbulent dynamo maintain a constant open flux carried to the heliosphere by the Sun's floor-like slow SW.

Unified Astronomy Thesaurus concepts: Solar magnetic fields (1503); Quiet Sun (1322); Solar dynamo (2001); Solar cycle (1487); Solar radio emission (1522); Solar-terrestrial interactions (1473); Slow solar wind (1873)

Supporting material: data behind figure

1. Introduction

For the last seven solar minima, the lowest monthly value of the quiet Sun's 10.7 cm radio flux ($F_{10.7}$) has been in a narrow range of 68.1 ± 1.7 solar flux units (1 sfu = 10^{-22} W m^{-2} Hz^{-1}; Covington 1969, 1979; Tapping 2013; White & Schonfeld 2018; Schonfeld et al. 2019).[5] Although $F_{10.7}$ and the sunspot number (S_N) are highly correlated, the lowest daily number of spots on the Sun for each of these minima is zero while the $F_{10.7}$ flux for spotless days during this interval ranges from 61 to 95 sfu. Clette (2021) recently considered daily $F_{10.7}$ values from 1947–2015 as a function of the number of contiguous spotless days on the Sun and showed that the mean value of $F_{10.7}$ for a spotless interval approaches a base level of 67 sfu asymptotically as the number of such days increases.[6]

$F_{10.7}$ is also highly correlated with the Sun's unsigned photospheric magnetic flux (Tapping et al. 2007; Henney et al. 2012; Svalgaard & Sun 2016). Schrijver et al. (2011) used a flux dispersal model based on the sunspot number and the Solar and Heliospheric Observatory (SOHO) Michelson Doppler Imager (MDI) observations to argue that a minimum state of the Sun's global magnetic activity (viz., a floor in the total unsigned flux of ∼1.5×10^{23} Mx) was approached during the deep solar minimum of 2008–2009. They noted that this minimum magnetic state is frequently observed locally in the quiet-Sun network between active region decay products and attributed the maintenance of such baseline network fields to the continual emergence of ephemeral regions (ERs) with unsigned fluxes of ∼10^{18} to a few times 10^{19} Mx. The emergence rate of these ERs shows little, if any, variation with the solar cycle (Hagenaar et al. 2008).

In agreement with Schrijver et al. (2011), Clette (2021) attributed the $F_{10.7}$ approach to 67 sfu at solar minimum to the gradual decay of the plage remnants of active regions which, after a prolonged spotless period, will allow the Sun to approach the minimal magnetic state of the quiet-Sun chromospheric network (Tapping & Zwaan 2001). If the 11 yr sunspot (22 yr magnetic) cycle were to disappear, the daily $F_{10.7}$ flux would be permanently at a floor level of ~67 sfu.

A floor has also been proposed for the magnetic field strength (B) in the solar wind (SW). From a ∼130 yr (1872–2004) reconstruction of SW B based on the geomagnetic interdiurnal variability index (IDV; Svalgaard & Cliver 2005), Svalgaard & Cliver (2007) argued for a ∼4.6 nT floor in B that was approached at each 11 yr solar sunspot minimum. However, this floor was immediately breached during the sunspot minimum between cycles 23 and 24 when annually averaged B values of 4.5 nT, 4.2 nT, and 3.9 nT were recorded for 2007, 2008, and 2009, respectively. This led Cliver & Ling (2011) to drop the yearly base

[5] $F_{10.7}$ (the solar radio flux at 2.8 GHz) data sources: https://www.ngdc.noaa.gov/stp/space-weather/solar-data/solar-features/solar-radio/noontime-flux/penticton/; https://omniweb.gsfc.nasa.gov/.

[6] Comparison of $F_{10.7}$ and sunspot number data (https://www.sidc.be/SILSO/datafiles) for the deep 2018–2019 minimum supports Clette's (2021) conclusion. The lowest monthly and daily values in the 1947–present $F_{10.7}$ series both occurred in 1954 (66.4 sfu for January and 61.6 sfu on November 3), with the lowest corresponding modern values occurring in October 2019 (67.0 sfu; 63.4 sfu on October 21).

Original content from this work may be used under the terms of the Creative Commons Attribution 4.0 licence. Any further distribution of this work must maintain attribution to the author(s) and the title of the work, journal citation and DOI.

level estimate of B to ∼2.8 nT (corresponding to an open solar flux of $\sim 8 \times 10^{21}$ Mx) based on extrapolations of two linear correlations: (i) a relation between SW B and solar polar field strength for the solar minima preceding cycles 21–24, and (ii) a precursor relation between the peak 11 yr cycle sunspot number and SW B at the preceding minimum for cycles 14–23.[7] In retrospect, the Svalgaard & Cliver (2007) floor of ∼4.6 nT was too high because it necessarily included a contribution from the variable polar fields at solar minimum—either directly from high-speed streams (HSSs) or indirectly via pressure balance—required for the observed continuation of the solar cycle (the underlying assumption of the precursor method, e.g., (ii) above; Svalgaard et al. 2005; Petrovay 2020) over the interval on which it was based.

Schrijver et al. (2011) concluded that the years 2008–2009 provided the best estimate of magnetic activity for the least active phases of the Maunder Minimum (MM; 1645–1715; Eddy 1976; Ribes & Nesme-Ribes 1993). In regard to SW B, Schrijver et al. (2011) attributed the SW in 2008–2009 to the polar coronal holes, while Cliver (2012) argued that the minimal magnetic state on the Sun inferred by Schrijver et al. (2011) was a prerequisite for the hypothesized floor in the SW.

In Section 2 we present evidence that $F_{10.7}$ is a proxy for the Sun's surface magnetism and compare how the magnetic field strength at the Sun's surface and in the SW approach their respective floor values at 11 yr cycle minima. In Section 3, we make conjectures based on these floors regarding (1) the existence of a turbulent small-scale dynamo (Durney et al. 1993; Petrovay & Szakaly 1993; Cattaneo 1999; Rempel et al. 2023) that produces a constant unsigned photospheric flux independently of the large-scale dynamo (Charbonneau 2020; Charbonneau & Sokoloff 2023) that produces the 11 yr cycle; and (2) the role of this small-scale dynamo in the generation of the floor-like slow SW (SSW). Our results are summarized and discussed in Section 4.

2. Comparative Magnetic Minima of the Sun and the Solar Wind

2.1. $F_{10.7}$ Is Highly Correlated with the Sun's Total Magnetic Flux

A comparison of the total magnetic flux on the solar disk (uncorrected for foreshortening), recorded by SOHO/MDI and the Solar Dynamics Observatory (SDO) Helioseismic and Magnetic Imager (HMI) from 1996 to 2016, with $F_{10.7}$ is shown in Figure 1 (adapted from Svalgaard & Sun 2016). The bottom traces show the good agreement between observed $F_{10.7}$ (red line; adjusted to 1 au to remove the annual variation in the Earth's orbit) and $F_{10.7}{}^{*}$ (dark blue), computed from its linear scaling to the Sun's total magnetic flux (MF) in the top trace.[8] The dashed line floor for $F_{10.7}$ is drawn at 67 sfu. The floor of $\sim 10^{23}$ Mx for the MF in the upper trace, corresponding to a $F_{10.7}$ value of 67 sfu, is substantial, representing about one-third of the total flux inferred for the maximum of sunspot cycle 19 (1954–1964; the largest cycle ever recorded) that had a peak monthly $F_{10.7}$ value of 281 sfu in 1957. The reconstruction of MF in Figure 1 is similar to that of Tapping et al. (2007) given in Figure 3 of Schrijver et al. (2011) that was based on the MF of the full Sun, with foreshortening taken into account, and a $F_{10.7}$ floor of 68 sfu, to yield a quasi-constant total flux value for the MM of $\sim 4.5 \times 10^{23}$ Mx versus $\sim 1.5 \times 10^{23}$ from Schrijver et al. (2011).

2.2. Differing Behavior of Solar and Solar Wind Magnetic Fields at Solar Minima

Figure 2 shows a marked difference in the relationship of annual averages of SW B and $F_{10.7}$ to their respective floors for recent solar cycles. The offset of SW B at solar minimum above the ∼2.8 nT floor (top panel) is more pronounced and variable than that of $F_{10.7}$ (bottom panel), which approaches its 67 sfu floor at each minimum.[9] The largest offset from the floor at solar minima for $F_{10.7}$ is only ∼2%–5% of the offset for adjacent maxima compared to ∼25%–50% for SW B.

The dashed line in Figure 3, an updated version of Figure 1 in Cliver & Ling (2011), shows that the offset of SW B above the ∼2.8 nT floor at each solar minimum is approximately proportional to the corresponding polar field strength. In addition to the B contribution from the polar coronal holes, this offset will include coronal mass ejection (CME)–associated contributions from low-latitude old-cycle and midlatitude new-cycle active regions as well as HSS contributions from their associated coronal holes. Reaching the floor would require the disappearance of the dipole field and, as a result, the 11 yr solar and SW cycle—a circumstance that did not occur even during the MM (Berggren et al. 2009).[10]

Figure 4 shows that the different ways in which SW B and $F_{10.7}$ approached their respective floors during the ∼50 yr interval in Figure 2 have persisted for ∼180 yr. The top panel gives SW B from 1845 to 2022, with the values through 1964 taken from the community-vetted B series of Owens et al. (2016) based on the IDV index. As a long-term proxy for $F_{10.7}$, Svalgaard (2016) and others have shown that $F_{10.7}$ is also highly correlated with the solar EUV emission that drives the diurnal geomagnetic variation parameterized by the daily range (in nT) of the magnetic East component (rY). Figure 4 (bottom panel) shows that for each solar minimum from 1840 to 2014, rY dropped close to its floor value of ∼33 nT, in contrast with SW B in the top panel. Svalgaard (2016) obtained

$$F_{10.7} = (rY/4)^2 \quad (1)$$

for the years 1996–2014. For rY = 33 nT at cycle minima, Equation (1) yields $F_{10.7} = 68$ sfu, close to the 67 sfu floor from Clette (2021).[11]

2.3. Decomposition of Solar Wind B into Contributions from Coronal Mass Ejections, High-speed Streams, and Slow Solar Wind for the Last ∼60 yr

Richardson et al. (2000) and Richardson & Cane (2012) separated the SW into its three principal components based on

[7] The concept of a floor in B is implicit in the "CME-less" ∼4.8 nT background SW field of Owens & Crooker (2006), subsequently lowered to ∼3.7 nT (Crooker & Owens 2010). Svalgaard (2020) also favors a floor value closer to ∼4 nT.

[8] MDI and HMI data source: http://jsoc.stanford.edu/.

[9] Figure 2 data sources: SW B, $F_{10.7}$ (https://omniweb.gsfc.nasa.gov/; https://www.ngdc.noaa.gov/stp/space-weather/solar-data/solar-features/solar-radio/noontime-flux/penticton/)

[10] Figure 3 data sources: dipole moments for cycles 22–25 (http://wso.stanford.edu/), for cycle 21 estimate (Svalgaard et al. 2005); SW B (https://omniweb.gsfc.nasa.gov/).

[11] Figure 4 data sources: SW B for 1845–1964 from Supplementary Data in Owens et al. (2016) https://agupubs.onlinelibrary.wiley.com/doi/full/10.1002/2016JA022529) and after 1964 from https://omniweb.gsfc.nasa.gov/; rY data from Table 2 in Svalgaard (2016).

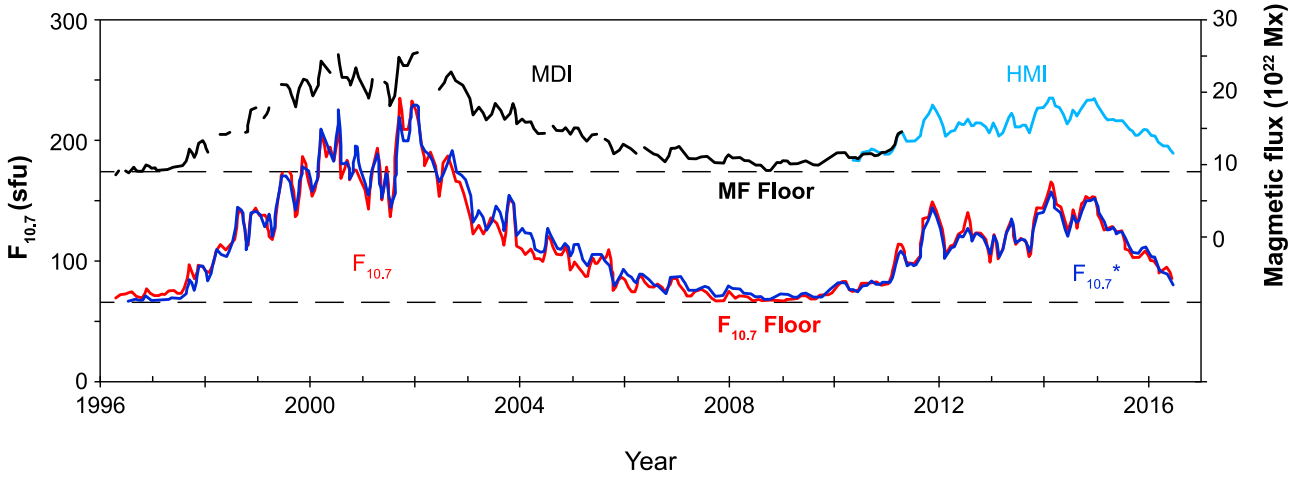

Figure 1. Upper curve: MDI line of sight (LOS) magnetic flux (MF; black) scaled to match the HMI LOS MF (light blue) based on their overlap. Lower curves: observed $F_{10.7}$ flux reduced to 1 au (red) and $F_{10.7}^{*}$ (dark blue), computed from the magnetic flux of the composite record. All curves have a 1 month resolution. (Adapted from Svalgaard & Sun 2016.)

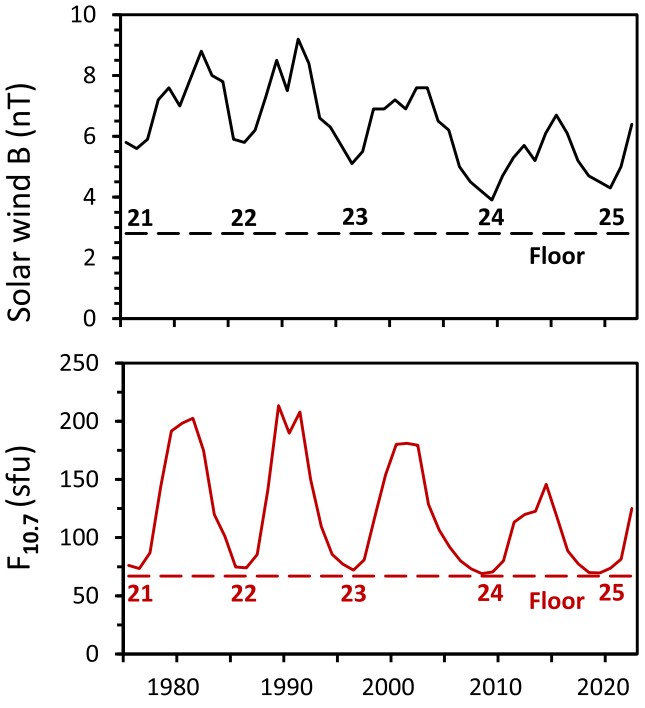

Figure 2. Top panel: annual values of solar wind B (1975–2022; solar cycles numbered) compared with a ∼2.8 nT floor. Bottom panel: yearly values of $F_{10.7}$ with a 67 sfu floor.

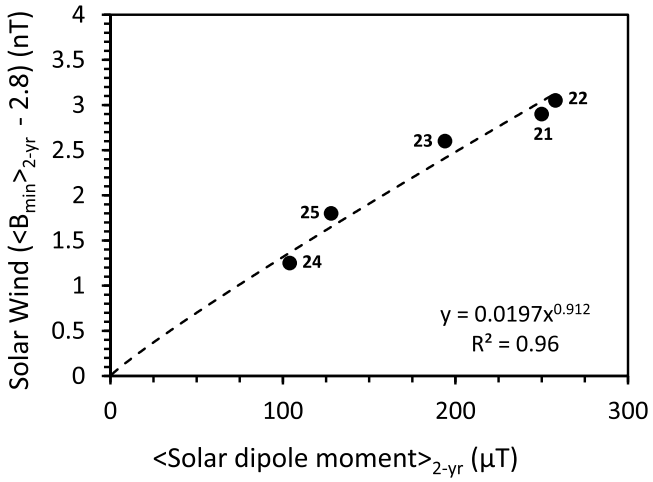

Figure 3. Power-law dependence of average solar wind B above a 2.8 nT floor (for the 2 yr with lowest $S_N(2.0)$ at solar minima for cycles 21–25) on the corresponding 2 yr averaged solar polar field strength (average unsigned difference between the northern and southern poles).

the various in situ signatures for each wind type: (1) CME-associated flows including CMEs—observed in situ via the characteristic signatures summarized by Zurbuchen & Richardson (2006)—and the sheaths of compressed ambient SW formed ahead of CMEs; (2) corotating HSSs (Richardson 2018); and (3) SSW—typically with speeds $\lesssim$400 km s^{-1}, relatively high densities and low proton temperatures, and a wide variation in plasma parameters. In the determination of flow types, use was made of geomagnetic index time series, solar energetic particle event records, and cosmic-ray modulation data to bridge some of the gaps in direct SW data, as discussed in Richardson & Cane (2012). A sample of this SW decomposition into its three components for an SSW dominated interval in 2009 is shown in Figure 5, and a listing of the annual contributions of the three principal SW components to SW B is given as the data behind Figure 6.

Panels ((a)–(c)) in Figure 6 show the contributions to average annual SW B at Earth from CMEs, HSSs, and SSW from 1965-2021, with sunspot number $S_N(2.0)$ (Clette et al. 2015; Clette & Lefevre 2016; Clette et al. 2023) plotted in panel (d).[12] The annual contribution to B for each flow type is the average field strength of that type during the year multiplied by the percentage of time Earth spent in the flow type. (Flows classified as "uncertain" (generally because of data gaps) are apportioned according to the percentage of time Earth was in each of the three principal flow types.) Panels (a) and (b) trace the solar cycle evolution of the SW. CMEs are the dominant contributor to SW B through the rise and peak of the cycle, with HSSs having their greatest impact on the decline of the cycle into solar minimum. At solar minimum HSSs and SSW make

[12] Figure 6 data sources: CME, HSSs, and SSW (see the data behind the figure); $S_N(2.0)$ (https://www.sidc.be/SILSO/datafiles). The detailed decomposition of the SW into the three principal flow types is available at Richardson (2023).

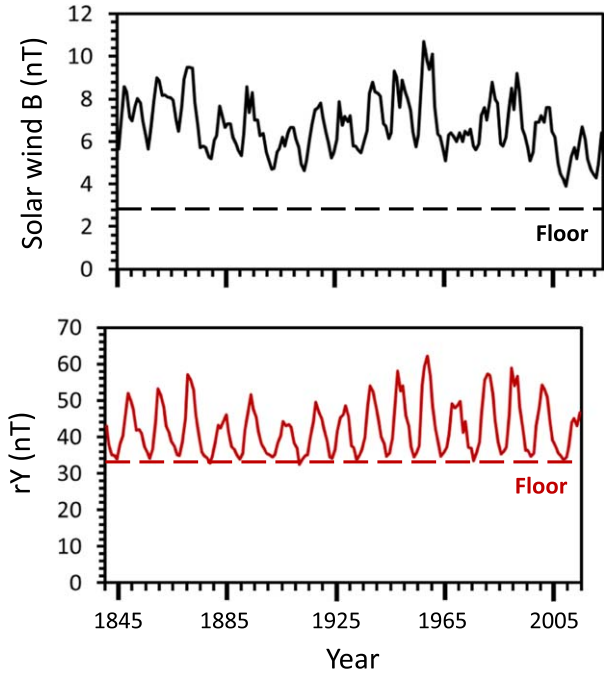

Figure 4. Top panel: annual solar wind B values (1845–2022; Owens et al. 2016) with a ∼2.8 nT floor indicated. Bottom panel: composite annually averaged diurnal geomagnetic variation rY showing the return to a ∼33 nT floor at each solar minimum from 1840 to 2014 (Svalgaard 2016).

approximately equal contributions of ∼2 nT. The constancy of the SSW B contribution through several solar cycles is remarkable, with the average value of 2.20 ± 0.44 nT approaching the estimated ∼2.8 nT floor.

The difference between the ∼2.8 nT floor obtained by Cliver & Ling (2011) and the ∼2.2 nT SSW contribution reflects uncertainties in the determination of both values. The SW floor in B is based on the linear extrapolation of two relationships. A contributing factor to the lower average SSW B value from Figure 6 is the occurrence of large late-cycle coronal holes that can dominate the solar wind in the ecliptic plane. The years 2008–2009 are instructive in this regard; from 2008 to 2009 the SSW contribution to SW B increased by ∼1 nT while the HSS contribution decreased by ∼1.5 nT after relatively large low-latitude coronal holes that were prominent through 2008 closed down (de Toma 2011). In 2009, Earth was in SSW flows ∼70% of the time (vs. ∼45% in 2008), with multiple intervals of SSW for ∼10–20 consecutive days (Figure 5). A second contributing factor to the lower average SSW B value in Figure 6 is the inclusion of the sheaths of compressed (typically slow) ambient SW formed ahead of CMEs in the CME component. The ∼60% reduction of average sunspot activity for the last 15 years (2007–2021) in panel (d) of Figure 6 relative to the preceding 1965–2006 interval was reflected in corresponding reductions of ∼60% and 30% of the CME and HSS contributions to SW B, respectively, vs. a 15% increase for the SSW toward the 2.8 nT floor.

3. Implications Based on Magnetic Floors at the Sun and in the Solar Wind

Based on the above analysis, we suggest that: (1) the Sun has a turbulent small-scale dynamo that is independent of the 11-yr (22-yr) cyclic dynamo; and (2) the quiet-Sun small-scale field generated by the turbulent dynamo is the source of the slow solar wind. Neither of these conjectures is new. The possibility of an independent small-scale dynamo was proposed theoretically several decades ago (see Rempel et al. 2023 for a review), with the hypothesized linkage of such a dynamo to the slow solar wind more recent (Cliver & Ling 2011; Cliver & von Steiger 2015). Both suggestions warrant revisiting because of the increasing evidence for the reality of solar and solar wind magnetic floors, which includes the support for a firm floor in $F_{10.7}$ (Clette 2021), the correlation of the Sun's total magnetic flux with $F_{10.7}$ (Figure 1), the contrasting behavior of observed/inferred solar surface and SW B above their respective floors over the last ∼180 yr (Figures 2 and 4), and the quasi-constancy of the SSW contribution to SW B during the last ∼60 yr (Figure 6), in contrast to the cyclic contributions of CMEs and HSSs. Additional support for these implications is provided by recent observations from SDO and Parker Solar Probe (PSP) (Bale et al. 2023; Raouafi et al. 2023).

3.1. Implication 1: Existence of a Small-scale Constant Dynamo that is Independent of the Large-scale Cyclic Dynamo

In a recent review of magnetic fields in the solar convection zone, Fan (2021) wrote: "The well-organized pattern and cycle dependence as described by the butterfly diagram, the Hale polarity rule, and Joy's law exhibited by active regions are progressively less well obeyed by the smaller bipoles. Small ERs [ephemeral regions] emerge in both the closed-field, mixed polarity quiet-Sun regions as well as the more unipolar coronal hole regions (e.g., Hagenaar et al. 2008). The nature and origin of ERs are not certain. The ER flux may originate close to the surface produced by a "local dynamo" due to small-scale convective motions near the surface (e.g., Cattaneo et al. 2003; Bercik et al. 2005; [Vögler & Schüssler 2007; Buehler et al. 2013;] Rempel 2014).[13] Alternatively, ERs may correspond to flux sheared off from emerging or decaying active region flux tubes." In their review of magneto-convection and small-scale dynamo action, Borrero et al. (2017) emphasized the importance of determining "whether IN [internetwork] magnetic fields do actually arise from a turbulent small-scale dynamo or are leftovers of the magnetic fields from decaying active regions, being spread out over the solar surface by advection due to supergranulation, meridional flow, and differential rotation."

In this study, we have directly addressed the question raised in the above reviews. The different ways in which the Sun's total magnetic flux and SW magnetic field strength approach their respective floors at 11 yr minima—as shown by direct observations over the last 50 yr (Figures 1 and 2) and proxy data for the ∼1840–1965 (Figure 4) interval—argue for the existence of two separate dynamos at the Sun: a time-varying cyclic dynamo (Charbonneau 2020) that generates the strong fields underlying large-scale magnetic features such as active regions and coronal holes that dominate the photospheric and SW magnetic flux at solar maximum and an independent constant small-scale turbulent dynamo (Rempel et al. 2023) that maintains a floor at all times in the Sun's surface magnetism and arguably in the SW as well (Section 3.2).

On the rise to the maximum of the solar cycle, the CMEs and HSSs driven by the surface magnetic flux generated by the

[13] It is likely that small-scale dynamo action occurs over a large fraction, if not all, of the convection zone (Parnell et al. 2009; Thornton & Parnell 2011; Rempel et al. 2023).

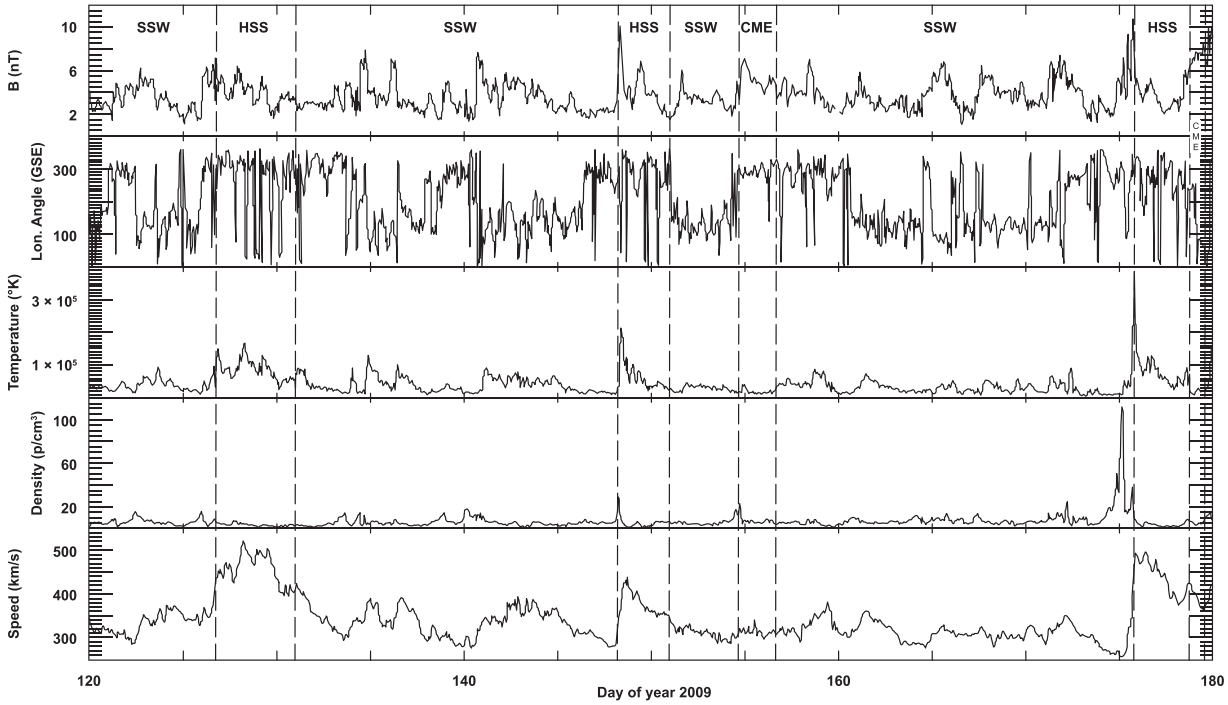

Figure 5. Example of the decomposition of the solar wind for the 60 days interval from 2009 April 30 to June 28 into its three principal components: coronal mass ejections (CME), high-speed streams (HSS), and slow solar wind (SSW). After Richardson et al. (2000) and Richardson & Cane (2012). Data sources: http://omniweb.gsfc.nasa.gov/; Richardson (2023).

large-scale dynamo lead to a corresponding flux buildup in the SW. Processes related to the disconnection of CMEs (Crooker et al. 2002; Webb & Howard 2012) and the closing down of coronal holes (Wang & Sheeley 2004; Heinemann et al. 2023 and references therein) prevent the long-term buildup of magnetic flux in the heliosphere. Figures 3 and 6 indicate that, at solar minimum, this removal of "old-cycle" flux from the SW is largely complete, with the excess B over the ∼2.8 nT floor attributed mainly to the new-cycle polar coronal holes (Figure 3).

In contrast to the variability of the magnetic activity driven by the large-scale dynamo both at the Sun and in the SW during the solar cycle, the unsigned photospheric flux attributed to the small-scale dynamo at solar minima adheres closely to a fixed level or floor when it is most clearly observed at 11 yr minima (bottom panels in Figures 2 and 4), with the relatively small departures attributed to old-cycle magnetic remnants (Schrijver et al. 2011; Clette 2021). The return of the $F_{10.7}$ flux (a proxy for the unsigned photospheric flux) to ∼67 sfu at the depths of the last five solar minima and the variation of the corresponding solar polar field strength—a key parameter of the large-scale dynamo—by a factor of ∼2.5 for these five minima (Figure 3) argues that the postulated small-scale dynamo is independent of the 11 yr (22 yr) sunspot (magnetic cycle), i.e., it is operating at all times. This implication is bolstered by Clette's (2021) empirical finding that the $F_{10.7}$ value of 67 sfu is approached asymptotically as the number of spotless days increases and the likelihood that deeper minima would imply weaker polar fields (Figure 3), increasing the variability range of the polar field strength at solar minima.

The inferred constant flux level produced by the small-scale dynamo of ∼15–45 × 10^{22} Mx is dwarfed by the replenishment rate (with commensurate loss rate) of 3 × 10^{25} Mx day^{-1} for small-scale features with fluxes in the range 10^{16}–10^{20} Mx (Thornton & Parnell 2011) and exceeds the 6 × 10^{21} Mx day^{-1} (Schrijver & Harvey 1994) brought to the surface by active regions at cycle maximum. Significantly higher global baseline magnetic fluxes of ∼4 × 10^{24} Mx (for ∼70 G at optical depth unity in the photosphere; Rempel et al. 2023) are indicated by quiet-Sun magnetic field studies that account for Zeeman cancellation (Danilovic et al. 2016a, 2016b) or use the Hanle effect (del Pino Alemán et al. 2018).

3.2. Implication 2: Origin of the Slow Solar Wind in the Quiet-Sun Small-scale Field Generated by the Turbulent Dynamo

The floor-like behavior of the SSW contribution to SW B over ∼60 yr in Figure 6 suggests that a floor in the Sun's surface magnetism produced by a nonvarying small-scale dynamo may be a sufficient as well as a necessary condition for the existence of a floor in SW B. The opposite movement of the contribution of the SSW to SW B in comparison with those for CMEs and HSSs during the decreased solar activity of the last 15 years is telling. Rather than all contributions decreasing in concert as one might suspect for a common cyclic dynamo origin, the SSW contribution increased toward the ∼2.8 nT floor as the Sun became more quiet, making it easier to disentangle the SSW from the cyclic SW components. The above observations suggest that the SSW is produced by the magnetic carpet of small-scale magnetic fields generated by the constant solar dynamo,[14] shedding light on a long-standing problem in solar physics noted by Antiochos et al. (2011) who wrote, " … the connection to the Sun of the slow, non-steady wind is far from understood and remains a major mystery." In

[14] The "magnetic carpet" (Title & Schrijver 1998) is a collective term for the small Sun's small-scale field following the pioneering research of Harvey & Martin (1973) and Livingston & Harvey (1975) on ephemeral regions and "inner network" fields (commonly referred to as internetwork or intranetwork fields today).

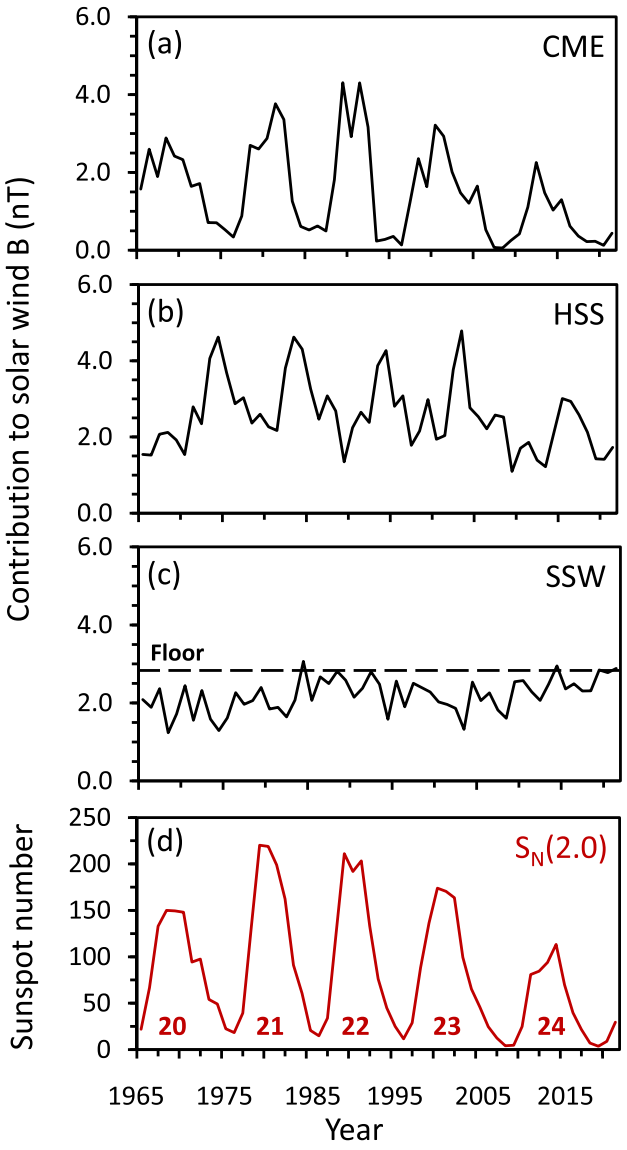

Figure 6. Decomposition of annually averaged solar wind B from 1965 to 2021 into its three components: (a) CME-related flows, (b) high-speed streams (HSSs), and (c) slow solar wind (SSW; with the ∼2.8 nT floor level indicated), for comparison with the sunspot number in panel (d), with cycle numbers indicated. The data behind this figure are available in machine-readable format.

(The data used to create this figure are available.)

the decade since this quote, interest in the origin of the SSW has only increased (Viall & Borovsky 2020). Cranmer et al. (2017) summarized the status of SSW research as follows: "Slow streams … appear to come from a wide range of sources, including streamers, pseudostreamers, coronal loops, active regions, and coronal hole boundaries." Not mentioned in this list of possible sources are quiet-Sun small-scale features (Bellot Rubio & Orozco Suárez 2019) such as supergranules and the internetwork.

Indirect support for an emphasis on a quiet-Sun small-scale field origin of SSW has recently been provided by PSP observations of switchbacks (Bale et al. 2019) and supergranular spatial scales (Bale et al. 2021; Fargette et al. 2021) in the SW and SDO observations of ubiquitous small-scale "jetlets" (Raouafi et al. 2023). Such observations led Bale et al. (2023) to attribute the Sun's fast SW to interchange reconnection (Crooker et al. 2002) involving network-scale magnetic elements in coronal holes, indirectly supporting implication 2 because the "reconnection/loop-opening" process based on interchange reconnection is often considered to be the generation mechanism for the SSW (Antiochos et al. 2011; Cranmer 2012). Bale et al. (2023) suggest that the primary difference between the acceleration of fast and slow SW may lie in the topology of the associated coronal hole.

4. Conclusion

4.1. Summary

A chain of proxies (solar $F_{10.7}$ flux to EUV flux to the geomagnetic rY parameter) indicates that the total photospheric magnetic flux has been essentially constant at solar minima over the last ∼180 yr, while corresponding SW B minimum values vary with the polar field strength (Figures 3 and 4). The Sun's unsigned flux at 11 yr minima is apparently independent of the measured polar field strength that varied by a factor of ∼2.5 over the last five minima. This discordance in magnetic behavior argues for two solar dynamos: the large-scale cyclic dynamo that dominates magnetic activity at the Sun and in the SW at solar maximum and an independent nonvarying small-scale turbulent dynamo that sets the floor level of the unsigned photospheric flux and SW B at all times. A decomposition of the SW into CMEs, HSSs, and SSW (Figure 6) indicates that the contribution of the SSW to SW B has been relatively constant over the last ∼60 yr, while those of CMEs and HSSs vary with the 11 yr cycle. The relative constancy of SSW B suggests an origin in an independent small-scale dynamo. Thus at each solar minimum, the heliosphere magnetic flux consists primarily of an HSS component attributed to the new-cycle polar coronal holes and an SSW floor. In sum, the evidence presented suggests the following picture: a small-scale nonvarying turbulent dynamo—that operates independently of the large-scale cyclic solar dynamo—generates a constant floor in the Sun's unsigned photospheric flux (with estimates of ∼1.5 and $\sim 4.5 \times 10^{23}$ Mx from Schrijver et al. 2011 and Tapping et al. 2007, respectively) that maintains a floor in SW open flux ($\sim 10^{22}$ Mx; Cliver & Ling 2011) that is carried by the SSW.

4.2. Discussion

Studies using modern instrumentation have also provided evidence for an independent turbulent dynamo. Buehler et al. (2013) and Lites et al. (2014) analyzed Hinode Spectro-polarimeter data for ∼6 yr intervals between 2006 and 2014 for quiet regions—at disk center and for all latitudes at central meridian, respectively—and found no measurable temporal variation of unsigned small-scale flux. Similarly, a synoptic program initiated at Locarno in 2007 based on spatially unresolved quasi-monthly observations with the Zimpol polarimeter has, at last report (Ramelli et al. 2019), detected no significant changes over time in Hanle depolarization of lines formed in the weakest fields of the quiet Sun.

Both Cliver & Ling (2011) and Schrijver et al. (2011) used the weak solar minimum years of 2008–2009 as a bridge to the MM. Even though the MM exhibited peculiar solar activity, with asymmetric (Ribes & Nesme-Ribes 1993) and extremely weak spottedness (Usoskin et al. 2015; Svalgaard & Schatten 2016), cosmogenic nuclide records indicate that the 11 yr

cycle continued throughout the ∼70 yr sunspot drought (Berggren et al. 2009). The associated weak polar fields would contribute to the MM SW. Extrapolations in Table 4 of Cliver & Ling (2011) suggest that the average SW speed and B at Earth during the MM would be in a floor-to-2009 range from 310 to 335 km s^{-1} and 2.8–3.9 nT, respectively (likely closer to the lower end of these ranges). It appears that, particularly at deep 11 yr minima and for the MM, the ubiquitous small-scale magnetic elements of the quiet Sun attributed to an independent turbulent dynamo play an important role in the magnetic flux budget of the SW as well as of the Sun itself.

As noted in Section 3.2, Bale et al. (2023) suggest that the primary difference between the acceleration of fast and slow SW may lie in the topology of the associated coronal hole. The most likely candidate for such a slow-wind coronal hole is the S-web (Antiochos et al. 2011; Baker et al. 2023). The S-web's conception was motivated by the broad latitudinal range of the SSW—up to the coronal polar holes at solar minima—and is supported by the extended temporal/longitudinal SSW flows (⩾10 days/>130°; presumably consisting of interleaved episodes of quiet radial flows and switchbacks; Bale et al. 2019; Fargette et al. 2021) at Earth in 2009 (Figure 5) when the solar surface was predominantly quiet.

Acknowledgments

E.W.C. thanks Leif Svalgaard and Sara Martin for helpful discussions. S.W. acknowledges support basic research from AFOSR. I.G.R. acknowledges support from the ACE mission. We thank the referee for helpful comments.

ORCID iDs

E. W. Cliver https://orcid.org/0000-0002-4342-6728
S. M. White https://orcid.org/0000-0002-8574-8629
I. G. Richardson https://orcid.org/0000-0002-3855-3634

References

Baker, D., Démoulin, P., Yardley, S. L., et al. 2023, ApJ, 950, 65
Bale, S. D., Badman, S. T., Bonnell, J. W., et al. 2019, Natur, 576, 237
Bale, S. D., Drake, J. F., McManus, M. D., et al. 2023, Natur, 618, 252
Bale, S. D., Horbury, T. S., Velli, M., et al. 2021, ApJ, 923, 174
Bellot Rubio, L., & Orozco Suárez, D. 2019, LRSP, 16, 1
Bercik, D. J., Fisher, G. H., Johns-Krull, C. M., & Abbett, W. P. 2005, ApJ, 631, 529
Berggren, A.-M., Beer, J., Possnert, G., et al. 2009, GRL, 36, L11801
Borrero, J. M., Jafarzadeh, S., Schüssler, M., & Solanki, S. K. 2017, SSR, 210, 275
Buehler, D., Lagg, A., & Solanki, S. K. 2013, A&A, 555, A33
Cattaneo, F. 1999, ApJ, 515, L39
Cattaneo, F., Emonet, T., & Weiss, N. O. 2003, ApJ, 588, 1183
Charbonneau, P. 2020, LRSP, 17, 4
Charbonneau, P., & Sokoloff, D. 2023, SSRv, 219, 35
Clette, F. 2021, JSWSC, 11, 2
Clette, F., Cliver, E. W., Lefèvre, L., Svalgaard, L., & Vaquero, J. M. 2015, SpWea, 13, 529
Clette, F., & Lefevre, L. 2016, SoPh, 291, 2629
Clette, F., Lefèvre, L., Chatzistergos, T., et al. 2023, SoPh, 298, 44
Cliver, E. W. 2012, in IAU Symp. 286, Comparative Magnetic Minima: Characterizing quiet times in the Sun and Stars, ed. C. H. Mandrini & D. F. Webb (Cambridge: Cambridge Univ. Press), 179
Cliver, E. W., & Ling, A. G. 2011, SoPh, 274, 285
Cliver, E. W., & von Steiger, R. 2015, SSR, 210, 227
Covington, A. E. 1969, JRASC, 63, 125
Covington, A. E. 1979, JRASC, 73, 1
Cranmer, S. R. 2012, SSR, 172, 145
Cranmer, S. R., Gibson, S. E., & Riley, P. 2017, SSR, 212, 1345
Crooker, N. U., Gosling, J. T., & Kahler, S. W. 2002, JGRA, 107, 1028
Crooker, N. U., & Owens, M. J. 2010, in ASP Conf. Ser. 428 Understanding a Peculiar Solar Minimum, ed. S. R. Cranmer, J. T. Hoeksema, & J. L. Kohl (San Francisco, CA: ASP), 279
Danilovic, S., van Noort, M., & Rempel, M. 2016a, A&A, 593, A93
Danilovic, S., Rempel, M., van Noort, M., & Cameron, R. 2016b, A&A, 594, A103
de Toma, G. 2011, SoPh, 274, 195
del Pino Alemán, T., Trujillo Bueno, J., Štěpán, J., & Shchukina, N. 2018, ApJ, 863, 164
Durney, B. R., De Young, D. S., & Roxburgh, I. W. 1993, SoPh, 145, 207
Eddy, J. A. 1976, Sci, 192, 1189
Fan, Y. 2021, LRSP, 18, 5
Fargette, N., Lavraud, B., Rouillard, A. P., et al. 2021, ApJ, 919, 96
Hagenaar, H. J., DeRosa, M. L., & Schrijver, C. J. 2008, ApJ, 678, 541
Harvey, K. L., & Martin, S. F. 1973, SoPh, 32, 389
Heinemann, S. G., Hofmeister, S. J., Turtle, J. A., et al. 2023, A&A, 679, A100
Henney, C. J., Toussaint, W. A., White, S. M., & Arge, C. N. 2012, SpWea, 10, S02011
Lites, B. W., Centeno, R., & McIntosh, S. W. 2014, PASJ, 66, S4
Livingston, W. C., & Harvey, J. 1975, BAAS, 7, 346
Owens, M. J., Cliver, E., McCracken, K. G., et al. 2016, JGRA, 121, 6048
Owens, M. J., & Crooker, N. U. 2006, JGR, 111, A10104
Parnell, C. E., DeForest, C. E., & Hagenaar, H. J. 2009, ApJ, 698, 75
Petrovay, K. 2020, LRSP, 17, 2
Petrovay, K., & Szakaly, G. 1993, A&A, 274, 543
Ramelli, R., Bianda, M., Berdyugina, S., Belluzzi, L., & Kleint, L. 2019, in ASP Conf. Ser., 526, Solar Polarization Workshop 8, ed. L. Belluzzi et al. (San Francisco: ASP), 283
Raouafi, N. E., Stenborg, G., Seaton, D. B., et al. 2023, ApJ, 945, 28
Rempel, M. 2014, ApJ, 789, 132
Rempel, M., Bhatia, T., Bellot Rubio, L., & Korpi-Lagg, M. J. 2023, SSRv, 219, 36
Ribes, J. C., & Nesme-Ribes, E. 1993, A&A, 276, 549
Richardson, I. G. 2018, LRSP, 15, 1
Richardson, I. G. 2023, Solar Wind Structure List Since 1963, v1, Harvard Dataverse, doi:10.7910/DVN/P4X3IZ
Richardson, I. G., & Cane, H. V. 2012, JSWSC, 2, A02
Richardson, I. G., Cliver, E. W., & Cane, H. V. 2000, JGR, 105, 18203
Schonfeld, S. J., White, S. M., Henney, C. J., Hock-Mysliwiec, R. A., & McAteer, R. T. J. 2019, ApJ, 884, 141
Schrijver, C. J., & Harvey, K. L. 1994, SoPh, 150, 1
Schrijver, C. J., Livingston, W. C., Woods, T. N., & Mewaldt, R. A. 2011, GRL, 38, L06701
Antiochos, S. K., Mikić, Z., Titov, V. S., Lionello, R., & Linker, J. A. 2011, ApJ, 731, 112
Svalgaard, L. 2016, SoPh, 291, 2981
Svalgaard, L. 2020, arXiv:2011.05356
Svalgaard, L., & Cliver, E. W. 2005, JGR, 110, A12103
Svalgaard, L., & Cliver, E. W. 2007, ApJ, 661, L203
Svalgaard, L., Cliver, E. W., & Kamide, Y. 2005, GRL, 32, L01104
Svalgaard, L., & Schatten, K. H. 2016, SoPh, 291, 2653
Svalgaard, L., & Sun, X. 2016, HMI Science Nuggets, 52. F10.7 Microwave Flux Matches the Total Disk Unsigned Magnetic Flux from MDI and HMI, http://hmi.stanford.edu/hminuggets/?p=1510
Tapping, K. F. 2013, SpWea, 11, 394
Tapping, K. F., Boteler, D., Charbonneau, P., et al. 2007, SoPh, 246, 309
Tapping, K. F., & Zwaan, C. 2001, SoPh, 199, 317
Thornton, L. M., & Parnell, C. E. 2011, SoPh, 269, 13
Title, A. M., & Schrijver, C. J. 1998, in ASP Conf. Ser. 154, The Tenth Cambridge Workshop on Cool Stars, Stellar Systems and the Sun, ed. R. A. Donahue & J. A. Bookbinder (San Francisco, CA: ASP), 345
Usoskin, I. G., Arlt, R., Asvestari, E., et al. 2015, A&A, 581, A95
Viall, N. M., & Borovsky, J. E. 2020, JGRA, 125, e26005
Vögler, A., & Schüssler, M. 2007, A&A, 465, L43
Wang, Y.-M., & Sheeley, N. R., Jr. 2004, ApJ, 612, 1196
Webb, D. F., & Howard, T. A. 2012, LRSP, 9, 3
White, S. M., & Schonfeld, S. 2018, AGUFM, 2018, SH43F–3724
Zurbuchen, T. H., & Richardson, I. G. 2006, SSR, 123, 31